*Graphical Abstract

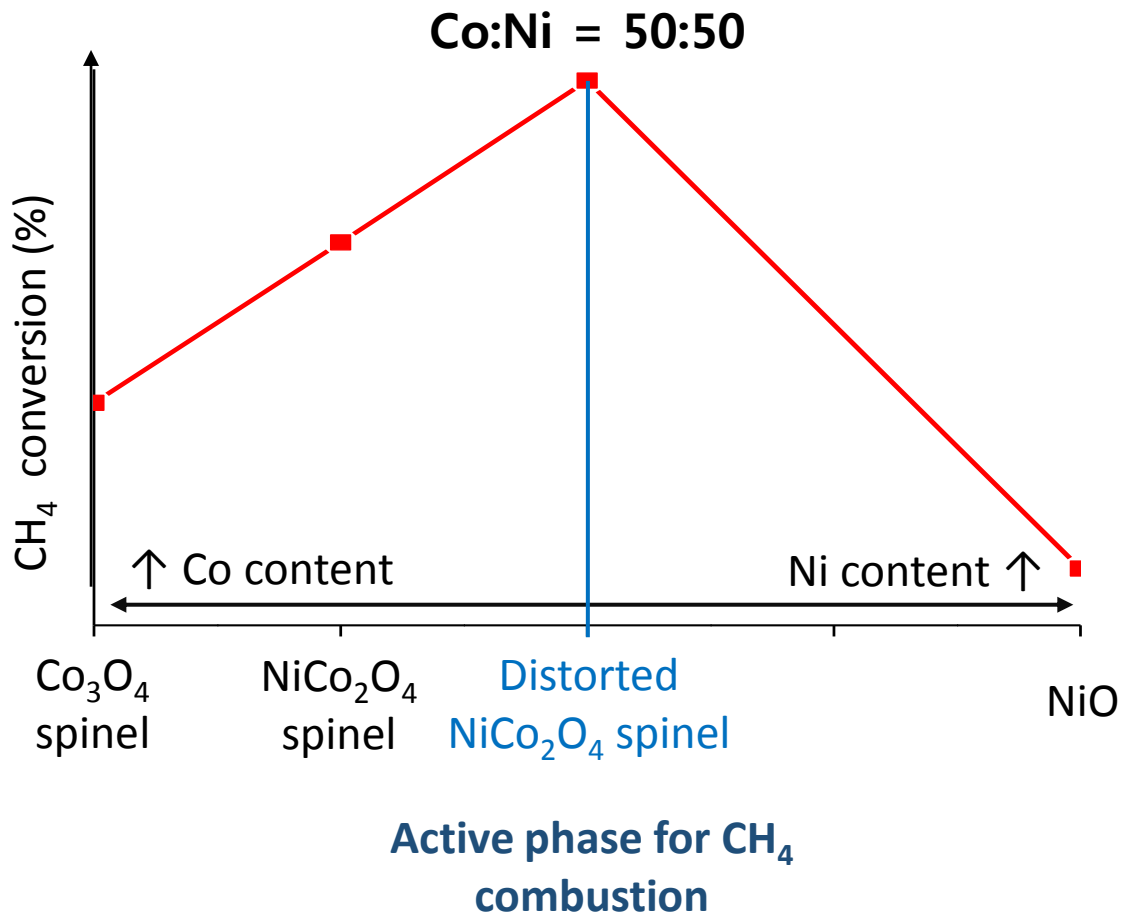

Effect of Co/Ni ratios in cobalt nickel mixed oxide catalysts on methane combustion

Tae Hwan Lim[a], Sung June Cho[b], Hee Sung Yang[c], M.H Engelhard[d], Do Heui Kim[a,*]

[a] School of Chemical and Biological Engineering, Seoul National University, 1 Gwanak-ro, Gwanak-gu, Seoul 151-742, Republic of Korea

[b] Clean Energy Technology Laboratory and Department of Applied Chemical Engineering, Chonnam National University, Gwangju, 500-757, Republic of Korea

[c] Environment Research Department / Advanced Technology Institute, Hyundai Heavy Industries CO., LTD., 1000 Bangeojinsunhwan-doro, Dong-gu, Ulsan 682-792, Republic of Korea

[d] Environmental Molecular Sciences Laboratory, Pacific Northwest National Laboratory, P.O. Box 999, Richland, WA 99354, United States

*E-mail address: dohkim@snu.ac.kr (D.H. Kim)

Abstract

A series of cobalt nickel mixed oxide catalysts with the varying ratios of Co to Ni, prepared by co-precipitation method, were applied to methane combustion. Among the various ratios, cobalt nickel mixed oxides having the ratios of Co to Ni of (50:50) and (67:33) demonstrate the highest activity for methane combustion. Structural analysis obtained from X-Ray Diffraction (XRD) and Extended X-ray Absorption Fine Structure (EXAFS) evidently demonstrates that CoNi (50:50) and (67:33) samples consist of $NiCo_2O_4$ and NiO phase and, more importantly, $NiCo_2O_4$ spinel structure is largely distorted, which is attributed to the

insertion of Ni^{2+} ions into octahedral sites in Co_3O_4 spinel structure. Such structural disorder results in the enhanced portion of surface oxygen species, thus leading to the improved reducibility of the catalysts in the low temperature region as evidenced by temperature programmed reduction by hydrogen (H_2 TPR) and X-ray Photoelectron Spectroscopy (XPS) O 1s results. They prove that structural disorder in cobalt nickel mixed oxides enhances the catalytic performance for methane combustion. Thus, it is concluded that a strong relationship between structural property and activity in cobalt nickel mixed oxide for methane combustion exists and, more importantly, distorted $NiCo_2O_4$ spinel structure is found to be an active site for methane combustion.

Keywords: Methane combustion; Cobalt nickel mixed oxide; $NiCo_2O_4$ spinel structure; EXAFS

1. Introduction

Methane is the most abundant hydrocarbon source on earth so that it can be used to substitute the petroleum-based fuel for transportation. For example, natural gas vehicles (NGVs) have attracted much attention as effective means of reducing emission of nitrogen oxides, hydrocarbons and carbon monoxide compared to gasoline and diesel vehicles, so that they become popular for urban transportation [1, 2]. However, unburned methane emitted from NGVs is potent greenhouse gas because its global warming potential is 21 times higher than that of carbon dioxide [3-5]. Hence, it is expected to regulate the emission of methane not only from NGVs but also from on-road engines. From the perspective of catalyst researcher, it is difficult to oxidize unburned methane at low temperature having the strongest C-H bond among hydrocarbons [6]. Therefore the efforts to reduce the emission of unburned methane become rather important.

Catalytic combustion of methane (CCM) has used either noble metal or transition metal oxides as catalyst. Noble metal (such as Pt, Pd) [7-10] catalysts demonstrate an excellent catalytic performance in CCM at low temperature, but they are limited in commercial application because of high price and rarity. Transition metal (such as Mn, Fe, Cu, Co, Ni, Cu etc.) [11-18] oxide catalysts have been receiving considerable attention to substitute for noble metal due to the economic reason. However, the intrinsic activity of transition metal oxide catalysts is much lower than that of noble metal catalysts. For this reason, the recent studies about the use of transition metal oxide catalysts for CCM have been focused on the enhancement of the catalytic performance to reach the level of noble metal based catalysts. Among transition metal oxides, cobalt oxide is known to be very active for methane oxidation as well as for carbon monoxide and propane oxidation [19-22]. Cobalt oxide

exhibits weak oxygen bond strength and high turnover frequency for redox reaction [23, 24]. Liotta et al. reported that the morphological and redox properties of cobalt cerium mixed oxides are strongly dependent on the Co/Ce ratio for methane combustion [25]. Li et al. claimed that a synergistic effect of cobalt manganese oxides with varying Co/Mn ratios is observed and, especially, Co/Mn ratio of 5/1 shows the superior performance for methane combustion [26]. In addition, Li et al. demonstrated that Co/Cr ratio of 1/2 displays the highest performance for methane combustion among the cobalt chromium mixed oxides due to the strongest adsorption of chemisorbed oxygen species [27]. Meanwhile, nickel oxide, a *p*-type semiconductor, contributes to the prominent defects such as cation vacancies and electron holes and is used in the various industrial fields due to its typical magnetic, electronic and catalytic properties [28]. Zhang et al. found that the oxygen mobility and reducibility in Mn-Ni mixed oxides are improved by high coordination number and certain nickel vacancies, especially at Mn/(Mn+Ni) ratio of 0.13 [29]. Chen et al. reported that Ni-Co mixed oxides have better catalytic performance than pure NiO and Co_3O_4 for carbon monoxide oxidation [30]. According to previous researches, it is anticipated that the suitable mixing of NiO with Co_3O_4 can achieve superior activity for methane combustion due to the desirable intrinsic property. However, to the best of our knowledge, there is no previous research about the application of cobalt nickel mixed oxides to methane combustion.

In this study, a series of cobalt nickel mixed oxides were prepared by co-precipitation method and applied to methane combustion reaction to oxidize unburned methane. N_2 adsorption-desorption with BET method, ICP-AES, XRD, XPS and EXAFS were applied to examine physical and structural property of cobalt nickel mixed oxides with various Co/Ni ratios, and H_2 TPR and XPS O 1s were used to investigate their reducibility and surface

adsorbed oxygen. Therefore we aimed at finding the optimized Co/Ni ratio having an outstanding synergism between Co_3O_4 and NiO, which eventually led to find the relationship between structural property and activity in cobalt nickel mixed oxide for methane combustion.

2. Experimental

2.1 Catalysts preparation

Cobalt nickel mixed oxides with the varying ratios of Co to Ni were prepared by co-precipitation method [31, 32]. In a typical preparation, Na_2CO_3 aqueous solution was added to drop by drop to the mixed aqueous solution of $Co(NO_3)_2 \cdot 6H_2O$ and $Ni(NO_3)_2 \cdot 6H_2O$ while stirring at 60 °C until pH reaches 9.3 ± 0.01. The resulting precipitate was aged at 60 °C for 4 h, then filtered and washed with distilled water several times, followed by drying at 100 °C overnight. The dried material was ground and calcined at 500 °C for 3 h. Catalyst with various Co/Ni ratios was designated as CoNi (ratio) in this manuscript.

2.2 Catalysts characterization

Surface area and pore volume of the catalysts were measured using N_2 adsorption-desorption method at -195.7 °C with a ASAP 2010 (Micromeritics). Prior to the measurement, all samples were degassed under evacuated condition at 250 °C for at least 5 h. The surface area and pore volume of the samples were calculated using BET and BJH method, respectively.

Inductively coupled plasma-atomic emission spectroscopy (ICP-AES), Optima-4300 DV (PerkinElmer) was used to obtain an actual atomic Co/Ni ratio of the catalysts. Prior to the

analysis, 40 mg of each samples was dissolved in aqua regia which was composed of 1.25 mL of concentrated nitric acid and 3.75 mL of concentrated hydrochloric acid.

Crystal structure of the catalysts was examined using the powder X-Ray Diffraction (XRD). XRD analysis was carried out on a Smart Lab (Rigaku) with Cu Kα radiation at 50 mA and 40 kV. The operating conditions such as the step size of 0.02° at scan rate of 0.1°/min from 15° to 90° allow us to obtain the very fine XRD pattern. The crystal structure parameters of the samples were calculated using the Materials Analysis Using Diffraction (MAUD) Rietveld refinement program [33].

Temperature programmed reduction by hydrogen (H_2 TPR) was applied to investigate the reducibility of the samples by detecting the hydrogen consumption using a thermal conductivity detector (TCD) in a BEL-CAT BASIC (BEL Japan Inc.). Prior to the reduction, the samples were pretreated at 400 °C for 1h in an argon flow of 30 mL/min and then cooled down to room temperature. After that, they were reduced with 5% H_2/Ar until the temperature reached 650 °C at the rate of 10 °C/min.

X-ray Photoelectron Spectroscopy (XPS) analysis was conducted in a Quantum 2000 Scanning ESCA Microprobe (Physical Electronics). The instrument uses a focused monochromatic Al Kα X-ray (1486.7 eV) source operated at 100 W and 100 μm-diameter beam. The binding energy scale was calibrated using the carbon C 1s at 284.6 eV for known standards. The de-convolution of XPS peak was performed with CasaXPS program.

Extended X-ray Absorption Fine Structure (EXAFS) was applied to examine the atomic structure. EXAFS spectrum was obtained on a R-XAS (Rigaku). Co and Ni K-edge EXAFS spectra of the samples were measured in the energy range of 7.5-8.7 keV and 8.0-9.3 keV, respectively. The obtained EXAFS data were analyzed by ATHENA and ARTEMIS following the literature [34].

2.3 Methane combustion reaction

The methane combustion reaction was conducted in a fixed-bed quartz reactor. The samples were blended with α-Al_2O_3 bead to dissipate the heat caused by the reaction. The reactants containing 1500 ppm CH_4, 12.12 vol% O_2 and balancing N_2 was applied to the catalysts bed via mass flow controllers (MKS) at a gas hourly space velocity (GHSV) of 60,000 h^{-1}.

Activity data were obtained at steady state condition from 200 °C to 550 °C while increasing the temperature by 50 °C. The reactants and reaction products were analyzed by an on-line gas chromatograph (Agilent 6890N) equipped with a packed column (Supelco 12390-U) and a thermal conductivity detector.

3. Results and Discussion

3.1 ICP-AES and BET results

ICP-AES, BET surface area and pore volume results of cobalt nickel mixed oxides with various Co to Ni ratios are summarized in Table 1. The ICP-AES results clearly show that an actual atomic ratio of all the samples is well matched with that of nominal loading.

As shown in Table 1, the surface area and pore volume of cobalt oxide are 35 m^2/g and 0.19 cm^3/g respectively, while those of nickel oxide are 31 m^2/g and 0.20 cm^3/g, indicating that theses single oxides have similar physical properties. When it comes to cobalt nickel mixed oxides, they have higher surface area and pore volume than each single oxide. In particular, CoNi (50:50) catalyst exhibits the highest surface area of 56 m^2/g and the largest pore volume of 0.33 cm^3/g among the catalysts. Previous reports on Co-Ce [25] and Co-Cr [27] have shown a similar tendency meaning that mixed oxides have the higher surface area than single oxides. On the other hand, Gou et al. reported that the surface area is the highest when cobalt

content is below 20% in cobalt nickel mixed oxide catalysts. Such a difference of surface area originates from different preparation method and calcination condition [30].

3.2 XRD results

Fig. 1 displays the XRD patterns of cobalt nickel mixed oxides with various Co/Ni ratios. The peaks in XRD patterns of cobalt oxide and nickel oxide samples are accurately assigned to Co_3O_4 phase (JCPDS 43-1003) and NiO phase (JCPDS 47-1049), respectively. For the case of cobalt nickel mixed oxides (b-e), both $NiCo_2O_4$ phase (JCPDS 20-0781) and NiO phase exist together. However, it is quite difficult to differentiate between Co_3O_4 and $NiCo_2O_4$ phase because they have same spinel structure with little difference in lattice parameter (Co_3O_4: 8.084 Å, $NiCo_2O_4$: 8.110 Å). Thus, in-depth investigation of lattice parameter in XRD patterns of these samples is rather important to confirm the presence of $NiCo_2O_4$ phase [35].

The lattice parameter, phase wt% and crystalline size are obtained from the Rietveld refinement of the XRD patterns, as listed in Table 2. Note that the value of phase wt% is quantitatively estimated using relative peak intensity ratio [36, 37]. All the catalysts are classified into three different types of crystal structure according to the major phase in the sample: NiO based type (Nickel oxide and 33:67), $NiCo_2O_4$ based type (50:50, 67:33 and 75:25) and Co_3O_4 based type (Cobalt oxide). Theoretically, CoNi (67:33) should form 100 wt% $NiCo_2O_4$ phase; however, it contains the mixture of 78 wt% $NiCo_2O_4$ phase and 22 wt% NiO phase based on the MAUD analysis. The formation of NiO phase orginates from the thermal decomposition of $NiCo_2O_4$ spinel phase above 400 °C during calcination process [38-40].

In order to analyze the detailed change in lattice parameter of the $NiCo_2O_4$ phase, the zoom in figure in the region of 35°-40° is shown in the right side of Fig. 1. The shift of the

diffraction peak toward low angle is observed with increasing nickel content from 25% to 50%. Especially, CoNi (50:50) and (67:33) sample are largely shifted to lower angle, resulting in the larger lattice parameter (8.125 Å and 8.120 Å) than that of reference (8.110 Å), respectively. Such an increment in the lattice parameter can be attributed to the insertion of Ni^{2+} ions into octahedral sites in Co_3O_4 spinel structure because the ion radius of Ni^{2+} (0.069 nm) is larger than that of Co^{3+} (0.055 nm) [41]. Although the previous studies suggest that the diffraction peak may be shifted to lower angle owing to thermal decomposition of $NiCo_2O_4$ spinel phase, we exclude the possibility because calcination condition is fixed in this study [37, 42].

Both XRD and BET results show the close relationship between structure and physical property in the various cobalt nickel mixed oxides with different Co to Ni ratio. Surface area of $NiCo_2O_4$ based samples is higher than that of Co_3O_4 and NiO based ones. When nickel content increases from 25% to 50%, the diffraction peak of $NiCo_2O_4$ phase becomes broad and crystalline size decreases, and distorted $NiCo_2O_4$ phase is formed. Thus, it indicates the formation of less crystalline structure which can account for the excellent physical property of the CoNi (50:50) sample. However, as nickel content exceeds 50%, the crystalline NiO phase becomes dominant, resulting in the decrease of surface area.

3.3 EXAFS results

EXAFS spectra of Co K-edge and Ni K-edge are used to obtain information about the coordination number (CN) of atomic pairs and the distance of surrounding atomic species. As demonstrated in Fig. 2, the Co K-edge and Ni K-edge EXAFS results indicate three main peaks and two main peaks below 4 Å, respectively. It is important that a typical value of 0.3-0.4 Å must be added to the radial distance to obtain real atomic bond distance because there

is no correction in the phase shift for radial distances in Fig. 2. The real atomic bond distance obtained after fitting with ARTEMIS is summarized in Table 3.

In Fig. 2(a), the three peaks of Co K-edge spectra at around 1.5 Å, 2.5 Å and 3 Å signify the atomic distance of Co-O, octahedral Co - octahedral Co (Co_{oct}-Co_{oct}) and octahedral Co - tetrahedral Co (Co_{oct}-Co_{tet}) respectively. In Fig. 2(b), the two peaks of Ni K-edge spectra at about 1.7 Å and 2.5 Å mean the atomic distance of Ni-O and octahedral Ni - octahedral Ni (Ni_{oct}-Ni_{oct}) respectively [43, 44].

As presented in Table 3, the CN value of the Co-O decreases from cobalt oxide to CoNi (50:50), while that of the Ni-O increases from CoNi (75:25) to nickel oxide. This phenomenon evidently demonstrates the preferential insertion of nickel species into octahedral sites in Co_3O_4 spinel structure, resulting in the formation of the tetrahedrally coordinated cobalt species in $NiCo_2O_4$ spinel structure [35, 45].

It is interesting to note that the atomic distance of Ni_{oct}-Ni_{oct} is shifted toward high distance when the nickel loading increases from 25% to 50% in Ni K-edge spectra (about 2.5 Å). Such shift is clearly caused by the difference in ion radius between Ni^{2+} and Co^{3+} since Ni^{2+} ions are mainly inserted into octahedral sites in Co_3O_4 spinel structure, as observed in XRD pattern. In addition, Windisch et al. reported that inserted Ni^{2+} ions into octahedral sites would cause structural distortion, as evidenced by the shift of Raman band to lower frequencies [46]. Note that Co_3O_4 has a normal spinel structure of AB_2O_4 type which consists of Co^{2+} ions and Co^{3+} ions occupying the tetrahedral sites and the octahedral sites, respectively [47-49]. Thus, EXAFS results evidently verify that most Ni^{2+} ions are primarily inserted into the octahedral sites in Co_3O_4 spinel structure, while the portion of Co^{3+} ions occupying the octahedral sites decreases.

3.4 XPS results

XPS spectra are applied to obtain the information on the oxidation state of each element on the surface. O 1s, Co 2p and Ni 2p photoelectron spectra for cobalt nickel mixed oxides with various Co/Ni ratios are shown in Fig. 3.

As indicated in Fig. 3(a), O 1s spectra of the catalysts can be de-convoluted to the main peak and shoulder peak referred to as O_α and O_β, respectively. The O_α component at lower binding energy (528.7-529.2 eV) is assigned to lattice oxygen and the O_β component at higher binding energy (530.5-530.7 eV) is assigned to surface adsorbed oxygen such as surface OH group, chemisorbed oxygen and part of surface oxyhydroxides [50-52]. If O_β/O_α ratio sets as standard for portion of surface adsorbed oxygen to lattice oxygen, surface adsorbed oxygen increases with increasing O_β/O_α ratio at the catalyst surface [26, 29]. As listed in Table 4, the descending order of O_β/O_α ratio is as follows: CoNi (50:50) > CoNi (67:33) > CoNi (75:25) > Nickel oxide ≈ CoNi (33:67) > Cobalt oxide. Catalysts having $NiCo_2O_4$ phase exhibit higher O_β/O_α ratio than other structure phases. Especially, CoNi (50:50) and (67:33) catalyst containing distorted $NiCo_2O_4$ phase have the highest O_β/O_α ratio among the cobalt nickel mixed oxides, which can contribute to enhancement of catalytic oxidation activity due to the higher amount of reactive surface adsorbed oxygen [53-55].

Fig. 3(b) shows that Co 2p spectra of the catalysts are fitted to two main peaks of Co $2p_{3/2}$ and Co $2p_{1/2}$ with binding energy at 779.9 and 795.0 eV in addition to two weak shakeup satellites. Co 2p peak intensity is proportional to cobalt content in cobalt nickel mixed oxides. In other words, it is clearly confirmed that bulk and surface concentration of cobalt display a similar tendency with varying cobalt content. To investigate oxidation state of cobalt surface species, Co $2p_{3/2}$ spectra are de-convoluted into two spin-orbit doublet of Co^{3+} and Co^{2+} component with binding energy at 779.1 and 780.8 eV [56-59]. The ratios of Co^{3+}/Co^{2+} are

used to measure the extent of inserted Ni^{2+} ions into octahedral sites in Co_3O_4 spinel structure. As presented in Table 4, the ratios of Co^{3+}/Co^{2+} decrease as follows: Cobalt oxide > CoNi (75:25) > CoNi (67:33) > CoNi (50:50) ≈ CoNi (33:67). The decrement in Co^{3+} ions continues with increasing nickel content and, finally, Co^{3+}/Co^{2+} ratio becomes constant after CoNi (50:50) catalyst. Thus, CoNi (50:50) catalyst has a similar Co^{3+}/Co^{2+} ratio like CoNi (33:67), which seemed to be saturated with Ni^{2+} ions on octahedral sites. Although CoNi (50:50) and CoNi (33:67) catalyst have a quite similar Co^{3+}/Co^{2+} ratio, the phases observed in these XRD patterns are rather different because CoNi (50:50) has the distorted $NiCo_2O_4$ phase and CoNi (33:67) catalyst has the NiO phase. When nickel content exceed 50%, extra Ni^{2+} ions are not inserted into octahedral sites anymore, only to form NiO phase, thus leading to change from $NiCo_2O_4$ based structure to NiO based one [30, 37].

3.5 H_2 TPR results

The H_2 TPR profiles of cobalt nickel mixed oxides with various Co/Ni ratios are indicated in Fig. 4, in addition to the α and β peak position and H_2 uptake as listed in Table 5. All cobalt containing samples display weak reduction peak at lower temperature and strong reduction peak at higher temperature denoted as α peak and β peak, respectively. The α and β peak of cobalt oxide from at 272 °C and 382 °C are corresponding to the successive reduction from Co^{3+} to Co^{2+} and from Co^{2+} to Co° [30, 60] respectively, while nickel oxide has the single peak at 354 °C which is attributed to the reduction of Ni^{2+} to Ni°. As presented in Table 5, all the Co_3O_4 and NiO are almost completely reduced to the Co° and Ni° since the H_2 uptakes of cobalt oxide and nickel oxide are 15.8 and 12.2 mmol/g, which are close to the theoretical value of 16.6 and 13.3 mmol/g, respectively.

As shown in Table 5, the α peak temperature decreases with increasing nickel content and CoNi (50:50) and (67:33) catalyst have the α peak temperature corresponding to 234 °C and 247 °C, respectively. In comparison to Co_3O_4, the α peak temperature of both catalysts is largely shifted toward low temperature. Here, the lower reduction temperature means that reducibility of the catalysts is enhanced so that they have superior reducibility among the cobalt nickel mixed oxides, which is closely related to the maximum O_β/O_α ratio of CoNi (50:50) obtained XPS O 1s results. Such enhancement of reducibility is expected to have a strong impact on oxidation reaction [26, 29].

3.6 Methane combustion activity

Fig. 5 shows light-off curves of methane combustion on the samples with various Co/Ni ratios. Temperature where methane combustion conversion reaches 90% (T_{90}) can be regarded as the criterion of the catalytic activity for methane combustion. T_{90} of cobalt oxide and nickel oxide is 506 °C and 505 °C, respectively. T_{90} of most cobalt nickel mixed oxides is lower than 500 °C. Therefore, catalytic activity of cobalt nickel mixed oxides more significantly improved than that of single oxides. Methane combustion activity of various Co/Ni ratio catalysts increases with increasing nickel content up to the level of CoNi (50:50) catalyst. Especially, CoNi (50:50) and CoNi (67:33) catalyst reach T_{90} at 466 °C and 468 °C, both of which show the highest activity among the cobalt nickel mixed oxides. Fig. 5 clearly indicates that descending order of activity is as follows: CoNi (50:50) ≈ CoNi (67:33) > CoNi (75:25) > Cobalt oxide ≈ Nickel oxide > CoNi (33:67). To compare CoNi (50:50) catalyst with some existing catalysts, light-off curves of methane combustion on several catalysts are shown in Fig. 6, and the surface area and T_{90} of several catalysts we prepared and ones from the reference are summarized in Table 6 [7, 25 and 27]. Although CoNi (50:50) catalyst

shows lower activity than noble metal catalyst (1wt% Pd/γ-Al_2O_3), it demonstrates higher activity than other transition metal oxide catalysts. Thus, CoNi (50:50) catalyst in this study is proved to be an effective alternative catalyst for noble metal catalyst.

Correlation between physical property and activity is evidently established for cobalt nickel mixed oxide by combining the activity measurement with characterization results. When nickel content increases from 0% to 25%, $NiCo_2O_4$ phase is formed because Ni^{2+} ions are inserted into octahedral sites in Co_3O_4 spinel structure, and activity is enhanced However, Co_3O_4 and CoNi (75:25) catalysts having Co_3O_4 or $NiCo_2O_4$ phase, respectively, show a crossover of the light-off curves on Fig. 5, especially in the region of 400-550 °C. It is assumed that the crossover is attributed to the weak thermal stability of Co_3O_4 or $NiCo_2O_4$ phase unlike CoNi (67:33) and (50:50) ones having distorted $NiCo_2O_4$ phase. When nickel content increases more up to 33%, $NiCo_2O_4$ phase is slightly distorted and activity is enhanced. When nickel content increases from 33% to 50%, $NiCo_2O_4$ phase is largely distorted because Ni^{2+} ions are maximally inserted into octahedral sites, resulting in the optimal $NiCo_2O_4$ and NiO phase content having superior activity among the cobalt nickel mixed oxides. When nickel content excessively increases up to 67%, however, NiO phase is mainly formed and activity decreases. On account of exceeding capacity of octahedral sites, extra Ni^{2+} ions mainly form NiO phase. It implies that decrement in activity can be caused by the surface coverage of $NiCo_2O_4$ by NiO phase, indicating that surface area decreases when NiO phase is dominant [39]. Increasing order of activity is as follows: NiO phase < Co_3O_4 phase < $NiCo_2O_4$ phase < distorted $NiCo_2O_4$ phase.

Ion distribution model of cobalt nickel mixed oxides can be expressed as $Co^{2+}{}_{tet}[Ni^{2+}Co^{3+}]_{oct}O_3^{2-}\cdot O^-$, which was proposed by King and Tsueng [62]. It suggests that some of the oxygen anions exist as O^- ions in order to balance the excess negative charge produced by the

inserted Ni^{2+} ions into octahedral sites with the decreasing number of Co^{3+} ions. In addition, they claimed that such oxygen state was primarily related to the surface oxides as excess adsorbed oxygen. To sum up, the insertion of Ni^{2+} ions into octahedral sites in Co_3O_4 spinel structure causes the formation of O^- ions at the surface and so the extent of inserted Ni^{2+} ions is proportional to that of adsorbed oxygen. According to our XPS O 1s and methane combustion reaction test results, the adsorption of surface oxygen species increases with increasing nickel content, and, especially, CoNi (50:50) and (67:33) catalyst containing distorted $NiCo_2O_4$ phase have superior adsorption of surface oxygen species as well as the highest activity. Also, H_2 TPR results indicate that the catalysts have the highest reducibility of $NiCo_2O_4$ among the Ni-Co mixed oxide phases. Thus, XPS O 1s, H_2 TPR and methane combustion reaction test results clearly confirm that the catalysts having distorted $NiCo_2O_4$ phase exhibit the superior activity, the higher portion of surface oxygen species and improved reducibility of $NiCo_2O_4$. Therefore, it can be summarized that a strong correlation exists between activity and physical property and, more importantly, that distorted $NiCo_2O_4$ phase demonstrates the highest methane combustion activity.

4. Conclusions

The effect of Co/Ni ratio with various nickel content on methane combustion is explained by methane combustion reaction test and various characterizations like N_2 adsorption-desorption with BET method, ICP-AES, XRD, EXAFS, XPS and H_2 TPR. According to methane combustion reaction test, CoNi (50:50) and (67:33) catalyst exhibit superior activity for methane combustion among the cobalt nickel mixed oxides. XRD results evidently demonstrate that CoNi (50:50) and (67:33) catalyst, as $NiCo_2O_4$ based type, are in the form of $NiCo_2O_4$ phase and NiO phase and $NiCo_2O_4$ spinel structure is largely distorted compared to

other catalysts. EXAFS results indicate that shift toward high distance is observed between CoNi (75:25) and (50:50), arising from the difference of ion radius between Ni^{2+} and Co^{3+} occupying on octahedral sites. XPS Co 2p results show that distortion of $NiCo_2O_4$ spinel structure can be impacted by extent of inserted Ni^{2+} ions into octahedral sites in Co_3O_4 spinel oxide. Combined structural analysis obtained from XRD and EXAFS clearly demonstrates that extent of inserted Ni^{2+} ions into octahedral sites is related to the formation of distorted $NiCo_2O_4$ spinel structure. In addition, such structural disorder is attributed to enhancement for the adsorption of surface oxygen species and reducibility of $NiCo_2O_4$, as evidenced by H_2 TPR and XPS O 1s results. Thus, it is concluded that structural disorder in $NiCo_2O_4$ phase plays an important role for the methane combustion.

In summary, both characterization and reaction results lead us to the conclusion that a strong correlation exists between activity and physical property and superior performance for methane combustion is shown on CoNi (50:50) and (67:33) catalyst which possess distorted $NiCo_2O_4$ spinel structure.

Acknowledgements

The research is supported by Environment Research Department / Advanced Technology Institute in Hyundai Heavy Industries CO., LTD. A portion of this work was performed in the Environmental Molecular Sciences Laboratory (EMSL) at the PNNL. The EMSL is a national scientific user facility and supported by the U.S. DOE's Office of Biological and Environmental Research. PNNL is a multi-program national laboratory operated for the U.S. DOE by Battelle Memorial Institute under Contract DE-AC06-76RLO 1830.

5. References

[1] P. Gélin, M. Primet, Applied Catalysis B: Environmental 39 (2002) 1-37.

[2] D. Ciuparu, M.R. Lyubovsky, E. Altman, L.D. Pfefferle, A. Datye, Catalysis Reviews 44 (2002) 593-649.

[3] P. Gélin, L. Urfels, M. Primet, E. Tena, Catalysis Today 83 (2003) 45-57.

[4] T.V. Choudhary, S. Banerjee, V.R. Choudhary, Applied Catalysis A: General 234 (2002) 1-23.

[5] J.K. Lampert, M.S. Kazi, R.J. Farrauto, Applied Catalysis B: Environmental 14 (1997) 211-223.

[6] M. Aryafar, F. Zaera, Catalysis Letters 48 (1997) 173-183.

[7] Y. Liu, S. Wang, D. Gao, T. Sun, C. Zhang, S. Wang, Fuel Processing Technology 111 (2013) 55-61.

[8] X. Wang, G. Lu, Y. Guo, L. Jiang, Y. Guo, C. Li, J Mater Sci 44 (2009) 1294-1301.

[9] H. Yoshida, T. Nakajima, Y. Yazawa, T. Hattori, Applied Catalysis B: Environmental 71 (2007) 70-79.

[10] J.H. Lee, D.L. Trimm, Fuel Processing Technology 42 (1995) 339-359.

[11] T. Machej, E.M. Serwicka, M. Zimowska, R. Dula, A. Michalik-Zym, B. Napruszewska, W. Rojek, R. Socha, Applied Catalysis A: General 474 (2014) 87-94.

[12] R. Dumitru, F. Papa, I. Balint, D.C. Culita, C. Munteanu, N. Stanica, A. Ianculescu, L. Diamandescu, O. Carp, Applied Catalysis A: General 467 (2013) 178-186.

[13] Z. Jiang, J. Yu, J. Cheng, T. Xiao, M.O. Jones, Z. Hao, P.P. Edwards, Fuel Processing Technology 91 (2010) 97-102.

[14] S. Thaicharoensutcharittham, V. Meeyoo, B. Kitiyanan, P. Rangsunvigit, T. Rirksomboon, Catalysis Communications 10 (2009) 673-677.

[15] J. Cheng, J. Yu, X. Wang, L. Li, J. Li, Z. Hao, Energy & Fuels 22 (2008) 2131-2137.

[16] M.M. Pakulska, C.M. Grgicak, J.B. Giorgi, Applied Catalysis A: General 332 (2007) 124-129.

[17] T.C. Xiao, S.F. Ji, H.T. Wang, K.S. Coleman, M.L.H. Green, Journal of Molecular Catalysis A: Chemical 175 (2001) 111-123.

[18] G. Comino, A. Gervasini, V. Ragaini, Z.R. Ismagilov, Catalysis Letters 48 (1997) 39-46.

[19] G. Salek, P. Alphonse, P. Dufour, S. Guillemet-Fritsch, C. Tenailleau, Applied Catalysis B: Environmental 147 (2014) 1-7.

[20] B. Solsona, T.E. Davies, T. Garcia, I. Vázquez, A. Dejoz, S.H. Taylor, Applied Catalysis B: Environmental 84 (2008) 176-184.

[21] F. Grillo, M.M. Natile, A. Glisenti, Applied Catalysis B: Environmental 48 (2004) 267-274.

[22] J. Jansson, A.E.C. Palmqvist, E. Fridell, M. Skoglundh, L. Österlund, P. Thormählen, V. Langer, Journal of Catalysis 211 (2002) 387-397.

[23] N. Bahlawane, Applied Catalysis B: Environmental 67 (2006) 168-176.

[24] I.E. Wachs, K. Routray, ACS Catalysis 2 (2012) 1235-1246.

[25] L.F. Liotta, G. Di Carlo, G. Pantaleo, A.M. Venezia, G. Deganello, Applied Catalysis B: Environmental 66 (2006) 217-227.

[26] J. Li, X. Liang, S. Xu, J. Hao, Applied Catalysis B: Environmental 90 (2009) 307-312.

[27] J. Chen, X. Zhang, H. Arandiyan, Y. Peng, H. Chang, J. Li, Catalysis Today 201 (2013) 12-18.

[28] S. Mrowec, Z. Grzesik, Journal of Physics and Chemistry of Solids 65 (2004) 1651-1657.

[29] Y. Zhang, Z. Qin, G. Wang, H. Zhu, M. Dong, S. Li, Z. Wu, Z. Li, Z. Wu, J. Zhang, T. Hu, W. Fan, J. Wang, Applied Catalysis B: Environmental 129 (2013) 172-181.

[30] Y. Gou, X. Liang, B. Chen, Journal of Alloys and Compounds 574 (2013) 181-187.

[31] G.J. Hutchings, R.G. Copperthwaitet, F.M. Gottschalk, R. Hunter, J. Mellor, S.W. Orchard, T. Sangiorgio, Journal of Catalysis 137 (1992) 408-422.

[32] B. Chi, J.B. Li, Y.S. Han, J.H. Dai, Materials Letters 58 (2004) 1415-1418.

[33] http://www.ing.unitn.it/~maud/.

[34] B. Ravel, M. Newville, Journal of Synchrotron Radiation 12 (2005) 537-541.

[35] C.F. Windisch, G.J. Exarhos, R.R. Owings, Journal of Applied Physics 95 (2004) 5435-5442.

[36] M. Cabo, E. Pellicer, E. Rossinyol, O. Castell, S. Suriñach, M.D. Baró, Crystal Growth & Design 9 (2009) 4814-4821.

[37] M. Cabo, E. Pellicer, E. Rossinyol, M. Estrader, A. Lopez-Ortega, J. Nogues, O. Castell, S. Surinach, M.D. Baro, Journal of Materials Chemistry 20 (2010) 7021-7028.

[38] P. Peshev, A. Toshev, G. Gyurov, Materials Research Bulletin 24 (1989) 33-40.

[39] D.P. Lapham, A.C.C. Tseung, J Mater Sci 39 (2004) 251-264.

[40] S. Verma, H.M. Joshi, T. Jagadale, A. Chawla, R. Chandra, S. Ogale, The Journal of Physical Chemistry C 112 (2008) 15106-15112.

[41] Y.E. Roginskaya, O.V. Morozova, E.N. Lubnin, Y.E. Ulitina, G.V. Lopukhova, S. Trasatti, Langmuir 13 (1997) 4621-4627.

[42] S. Verma, A. Kumar, D. Pravarthana, A. Deshpande, S.B. Ogale, S.M. Yusuf, The Journal of Physical Chemistry C 118 (2014) 16246-16254.

[43] J. Rosen, G.S. Hutchings, F. Jiao, Journal of Catalysis 310 (2014) 2-9.

[44] C. Nordhei, A.L. Ramstad, D.G. Nicholson, Physical Chemistry Chemical Physics 10 (2008) 1053-1066.

[45] M. Lenglet, R. Guillamet, J. Dürr, D. Gryffroy, R.E. Vandenberghe, Solid State Communications 74 (1990) 1035-1039.

[46] C.F. Windisch Jr, K.F. Ferris, G.J. Exarhos, S.K. Sharma, Thin Solid Films 420–421 (2002) 89-99.

[47] K. Omata, T. Takada, S. Kasahara, M. Yamada, Applied Catalysis A: General 146 (1996) 255-267.

[48] F. Švegl, B. Orel, I. Grabec-Švegl, V. Kaučič, Electrochimica Acta 45 (2000) 4359-4371.

[49] J.A.K. Tareen, A. Małecki, J.P. Doumerc, J.C. Launay, P. Dordor, M. Pouchard, P. Hagenmuller, Materials Research Bulletin 19 (1984) 989-997.

[50] M.W. Nydegger, G. Couderc, M.A. Langell, Applied Surface Science 147 (1999) 58-66.

[51] F.ç. Larachi, J. Pierre, A. Adnot, A. Bernis, Applied Surface Science 195 (2002) 236-250.

[52] A. La Rosa-Toro, R. Berenguer, C. Quijada, F. Montilla, E. Morallón, J.L. Vázquez, The Journal of Physical Chemistry B 110 (2006) 24021-24029.

[53] H. Li, G. Lu, Y. Wang, Y. Guo, Y. Guo, Catalysis Communications 11 (2010) 946-950.

[54] J. Chen, W. Shi, J. Li, Catalysis Today 175 (2011) 216-222.

[55] H. Li, G. Lu, D. Qiao, Y. Wang, Y. Guo, Y. Guo, Catalysis Letters 141 (2011) 452-458.

[56] G. Li, L. Li, J. Shi, Y. Yuan, Y. Li, W. Zhao, J. Shi, Journal of Molecular Catalysis A: Chemical 390 (2014) 97-104.

[57] J.F. Marco, J.R. Gancedo, M. Gracia, J.L. Gautier, E. Rios, F.J. Berry, Journal of Solid State Chemistry 153 (2000) 74-81.

[58] J.G. Kim, D.L. Pugmire, D. Battaglia, M.A. Langell, Applied Surface Science 165 (2000) 70-84.

[59] T.J. Chuang, C.R. Brundle, D.W. Rice, Surface Science 59 (1976) 413-429.

[60] M. Kang, M.W. Song, C.H. Lee, Applied Catalysis A: General 251 (2003) 143-156.

[61] J.P. Jacobs, A. Maltha, J.G.H. Reintjes, J. Drimal, V. Ponec, H.H. Brongersma, Journal of Catalysis 147 (1994) 294-300.

[62] W.J. King, A.C.C. Tseung, Electrochimica Acta 19 (1974) 493-498.

Table 1 ICP-AES (Co:Ni), surface area and pore volume of cobalt nickel mixed oxides with various Co/Ni ratios.

Catalyst	ICP-AES (Co:Ni)	Surface area (m^2/g)	Pore volume (cm^3/g)
Cobalt oxide	100:0	35	0.19
CoNi (75:25)	74:26	48	0.26
CoNi (67:33)	67:33	46	0.26
CoNi (50:50)	52:48	56	0.33
CoNi (33:67)	32:68	35	0.19
Nickel oxide	0:100	31	0.20

Table 2 Lattice parameter (a), phase amount (wt%) and crystalline size (D) value of the catalysts calculated by fitting the XRD patterns using MAUD Rietveld refinement program.

Catalyst	NiO		$NiCo_2O_4$			Co_3O_4		
	a (Å)	wt%	a (Å)	wt%	D^1 (nm)	a (Å)	wt%	D^1 (nm)
Nickel oxide	4.179	100	-	-	-	-	-	-
CoNi (33:67)	4.183	65	8.111	35	11	-	-	-
CoNi (50:50)	4.161	31	8.125	69	10	-	-	-
CoNi (67:33)	4.177	22	8.120	78	12	-	-	-
CoNi (75:25)	4.161	9	8.114	91	15	-	-	-
Cobalt oxide	-	-	-	-	-	8.088	100	23

[1] Crystalline size of $NiCo_2O_4$ or Co_3O_4 estimated by the Scherrer equation using the (311) diffraction peak.

Table 3 Fitting parameters extracted from (a) Co and (b) Ni K-edge EXAFS data analysis of cobalt nickel mixed oxides with various Co/Ni ratios.

(a) Co K-edge

Catalyst	Atomic Pair	CN	Distance (Å)
Co foil	Co-Co	12.0	2.50
Cobalt oxide	Co-O	5.8±0.5	1.91
	Co-Co	5.6±0.6	2.86
	Co-Co	7.2±0.8	3.36
CoNi (75:25)	Co-O	4.9±0.4	1.92
	Co-Co	5.5±0.8	2.87
	Co-Co	7.6±1.2	3.38
CoNi (50:50)	Co-O	3.6±0.3	1.91
	Co-Co	4.1±0.6	2.89
	Co-Co	5.5±0.9	3.38

(b) Ni K-edge

Catalyst	Atomic Pair	CN	Distance (Å)
Ni foil	Ni-Ni	12.0	2.49
Nickel oxide	Ni-O	5.2±1.1	2.07
	Ni-Ni	11.8±1.5	2.96
CoNi (50:50)	Ni-O	5.4±0.8	2.05
	Ni-Ni	11.0±1.1	2.95
CoNi (75:25)	Ni-O	3.8±1.0	2.01
	Ni-Ni	11.2±2.2	2.92

Table 4 XPS results for the O 1s and Co 2p of cobalt nickel mixed oxides with various Co/Ni ratios.

Catalyst	O 1s (eV)		O_β/O_α ratio	Co $2p_{3/2}$ (eV)		Co^{3+}/Co^{2+} ratio
	O_β	O_α		Co^{2+}	Co^{3+}	
Cobalt oxide	530.7	529.2	0.44	780.8	779.1	1.69
CoNi (75:25)	530.7	529.1	0.70	780.8	779.1	1.58
CoNi (67:33)	530.7	529.1	0.75	780.5	779.0	1.47
CoNi (50:50)	530.6	529.0	0.79	780.5	779.0	1.40
CoNi (33:67)	530.5	528.8	0.54	780.3	778.8	1.38
Nickel oxide	530.5	528.7	0.55	-	-	-

Table 5 Peak position and H_2 uptake of H_2 TPR profiles in cobalt nickel mixed oxides with various Co/Ni ratios.

Catalyst	Peak position (°C)		H_2 uptake (mmol/g-cat)			
	α	β	α	β	α + β	α + β, theory[1]
Cobalt oxide	272	382	3.6	12.2	15.8	16.6
CoNi (75:25)	257	374	3.0	11.9	14.9	15.8
CoNi (67:33)	247	370	2.3	11.7	14.0	15.5
CoNi (50:50)	234	355	2.1	11.8	13.9	15.0
CoNi (33:67)	251	369	1.0	12.1	13.1	14.4
Nickel oxide	-	354	-	12.2	12.2	13.3

[1] Theoretical H_2 uptake calculated by assuming the complete reduction of Co_3O_4 and NiO to Co° and Ni°, respectively.

Table 6 Surface area and T_{90} of several catalysts we prepared and ones from the reference.

Catalyst	Surface area (m^2/g)		Calcination condition	T_{90} (°C)		Reference
	This work	Ref.		This work	Ref.	
CoNi (50:50)	56	-	500, 3h	466	-	This work
1wt% Pd/γ-Al_2O_3	208	44	500, 2h	420	433	[7]
$Co_1Cr_2O_4$	32	39	700, 4h	512	464	[27]
30wt% Co_3O_4/CeO_2	43	31	650, 5h	567	585	[25]

Figures

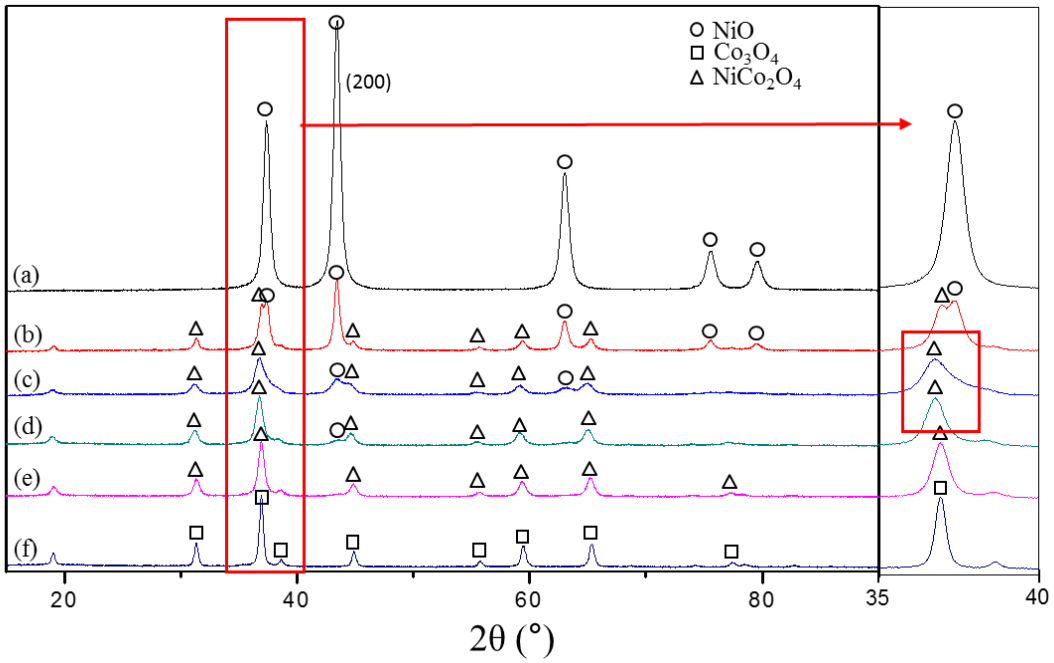

Fig. 1. XRD patterns of cobalt nickel mixed oxides: (a) Nickel oxide, (b) CoNi (33:67), (c) CoNi (50:50), (d) CoNi (67:33), (e) CoNi (75:25), (f) Cobalt oxide.

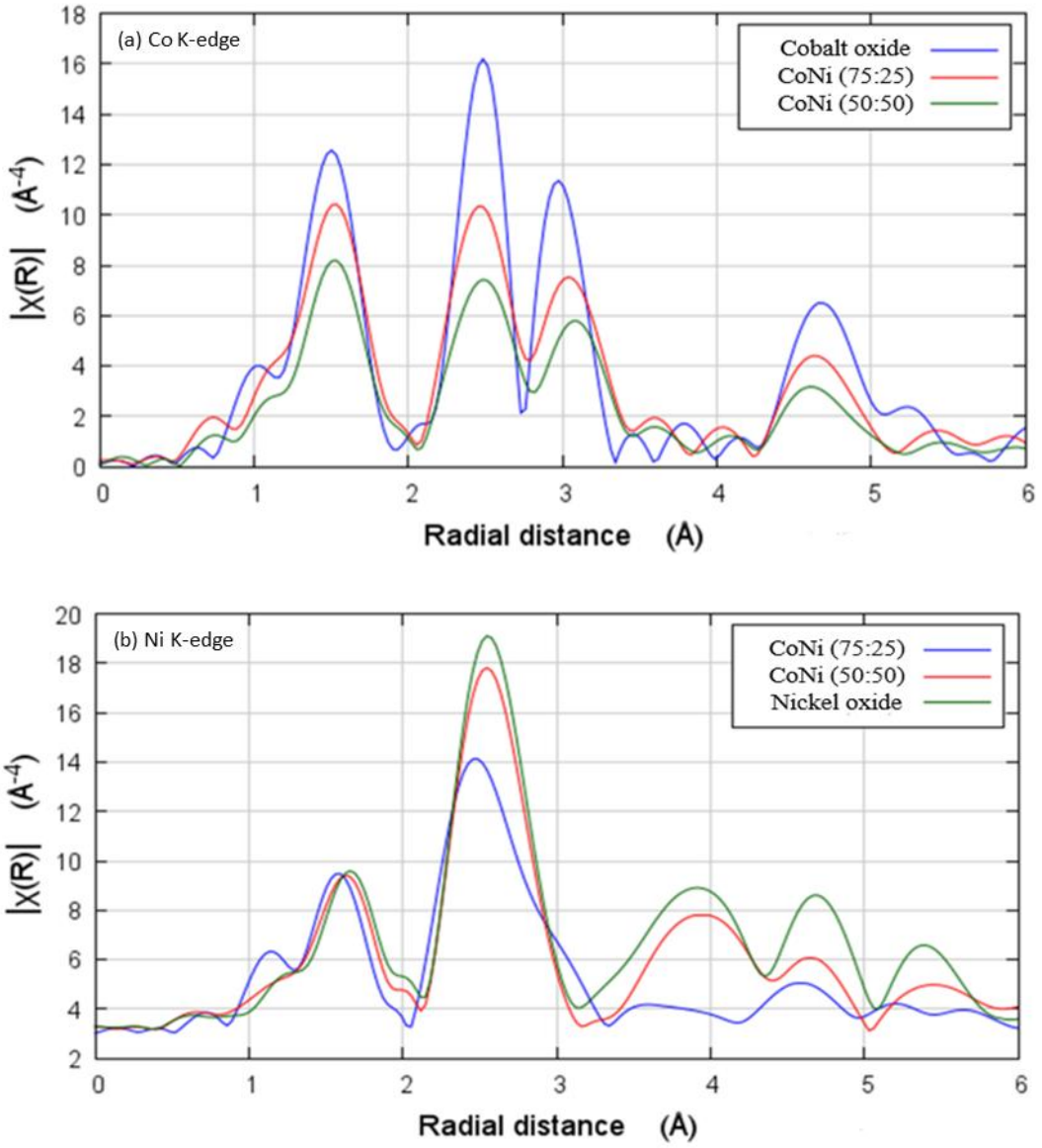

Fig. 2. (a) Co and (b) Ni K-edge EXAFS spectra of cobalt nickel mixed oxides with various Co/Ni ratios.

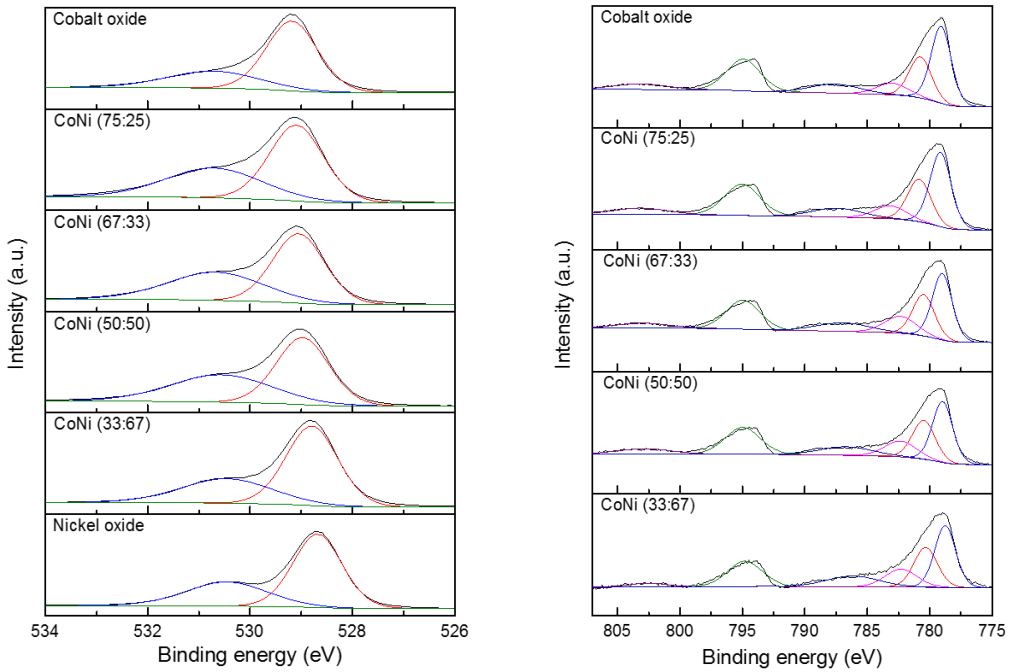

Fig. 3. XPS spectra for (a) O 1s, (b) Co 2p and (c) Ni 2p of cobalt nickel mixed oxides with various Co/Ni ratios.

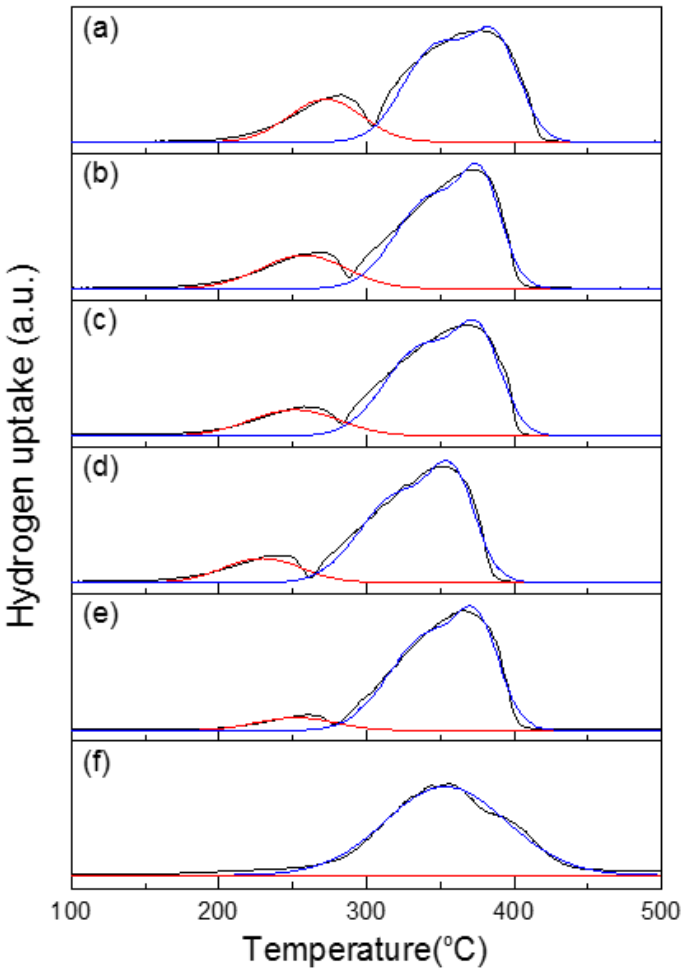

Fig. 4. H_2 TPR profiles of cobalt nickel mixed oxides with various Co/Ni ratios: (a) Cobalt oxide, (b) CoNi (75:25), (c) CoNi (67:33), (d) CoNi (50:50), (e) CoNi (33:67), (f) Nickel oxide.

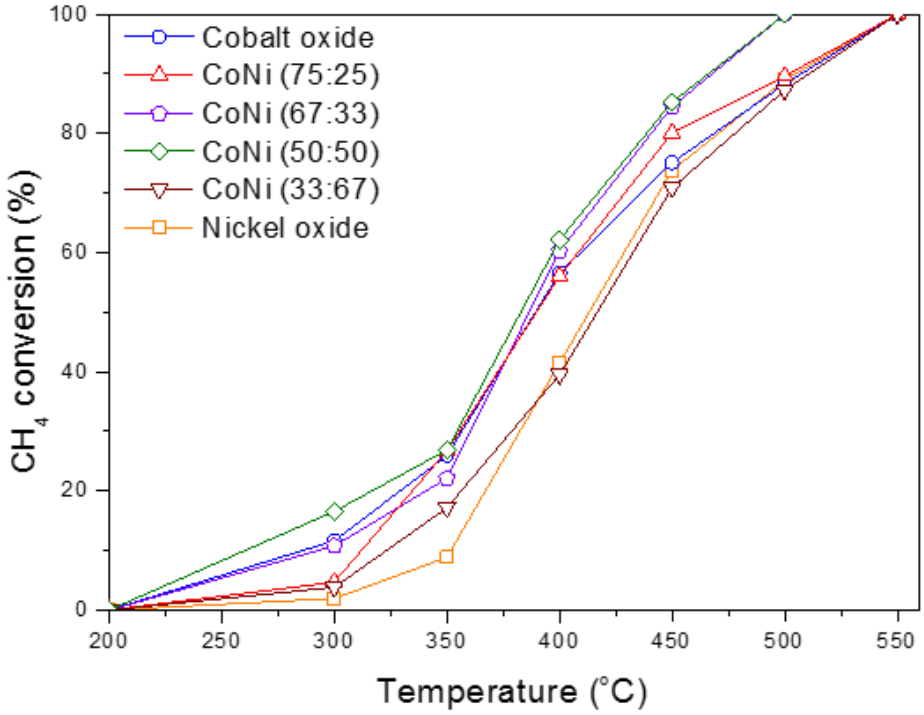

Fig. 5. Light-off curves of methane combustion on cobalt nickel mixed oxides with various Co/Ni ratios.

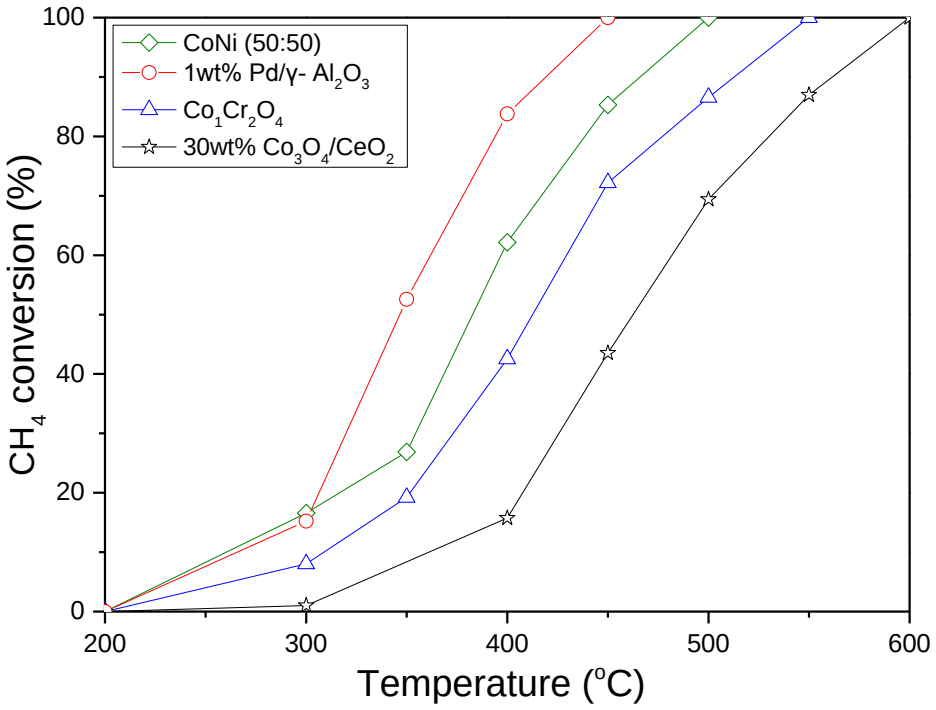

Fig. 6. Light-off curves of methane combustion on several catalysts.